

Cavity-soliton-enhanced mid-IR molecular sensing

Robert M. Gray,^{1*} Mingchen Liu,¹ Selina Zhou,¹ Arkadev Roy¹,
Luis Ledezma,^{1,2} and Alireza Marandi^{1†}

¹Department of Electrical Engineering, California Institute of Technology,
Pasadena, CA 91125, USA

²Jet Propulsion Laboratory, California Institute of Technology, Pasadena, CA 91109, USA

*Email: rmgray@caltech.edu

†Email: marandi@caltech.edu

Abstract

Optical molecular sensing is one of the most promising techniques for a wide range of applications, from fundamental studies to medical and environmental analysis. In the optical spectrum, the mid-infrared is particularly important for sensing because many molecules exhibit strong absorption features in this spectral region. To enhance the sensitivity of optical molecular sensing, typically passive and sometimes active cavities are used; however, these cavity-enhanced sensing techniques have so far faced fundamental trade-offs between sensitivity and dynamic range and practical challenges associated with the required cavity finesse and availability of laser gain materials. Here, we show that nonlinear dynamics in low-finesse resonators, namely the formation of quadratic cavity solitons, offer an enhancement mechanism for molecular sensing, which is not limited by these constraints. In proof-of-principle measurements of CO₂, we show an equivalent path length enhancement of nearly 2500. Additionally, we demonstrate large dynamic range through measurement of high concentrations of CO₂ with sensitivities that are orders of magnitude higher than those achievable through linear cavity-enhanced sensing, thereby breaking the fundamental limitations of standard optical sensing techniques.

There is great demand for the creation of molecular sensors exhibiting high sensitivity, reliability, specificity, and dynamic range for numerous applications. Optical sensors have emerged as leading candidates due to their reliability, sensitivity, and fast response times[19, 40]. The fundamental law governing linear absorption sensors, depicted in Fig. 1a, is the Beer-Lambert

Law, which says that the ratio of output power, P_{out} , to input power, P_{in} , for light which passes through a sample of length L with absorption coefficient α is given by $P_{out}/P_{in} = e^{-\alpha L}$. Some of the highest sensitivities in optical molecular sensing have been achieved through cavity-enhanced methods[32, 14, 36, 7, 33, 13]. Cavity-enhanced sensing in passive cavities occurs due to the prolonged interaction of light with a sample in high-finesse cavities, enabling the precise sensing and spectroscopy of trace gases [22].

Despite these numerous benefits, a known challenge in linear absorption sensing is an undesirable trade-off between the sensitivity and dynamic range, as shown in Fig. 1b. In particular, for a given optical power, one must sacrifice sensitivity at smaller sample concentrations to achieve high sensitivity at larger concentrations. Prior efforts to break this trade-off through cavity length multiplexing or simultaneous measurement of multiple absorption lines, while effective, result in increased system complexity and still are ultimately governed by this unfavorable exponential behavior. Specifically, such systems have a maximum achievable sensitivity that scales as the inverse of the absorption coefficient, indicated by the blue line in Fig. 1b (see Supplementary Information Section 3) [43, 27, 2, 39, 10].

Intracavity sensing in active cavities offers an alternative method for signal enhancement. These sensors benefit from the presence of a gain medium in the cavity and exploit near-threshold laser dynamics to achieve high sensitivities, even in the presence of broadband losses [3, 17]. Previous demonstrations of intracavity sensing have shown considerable enhancement in a variety of lasing systems including dye lasers[5, 37, 21], Ti:sapphire lasers[16], semiconductor lasers[6, 15], and fiber lasers[26, 41, 12, 35], among others[11, 30].

In the case where the spectral mode profile of the laser is narrower than the absorption line of interest, the sensor follows the single-mode theory for intracavity absorption sensing. Here, extremely large enhancement can be observed for measurements performed close to the laser threshold, asymptotically approaching infinity if spontaneous emission is not considered

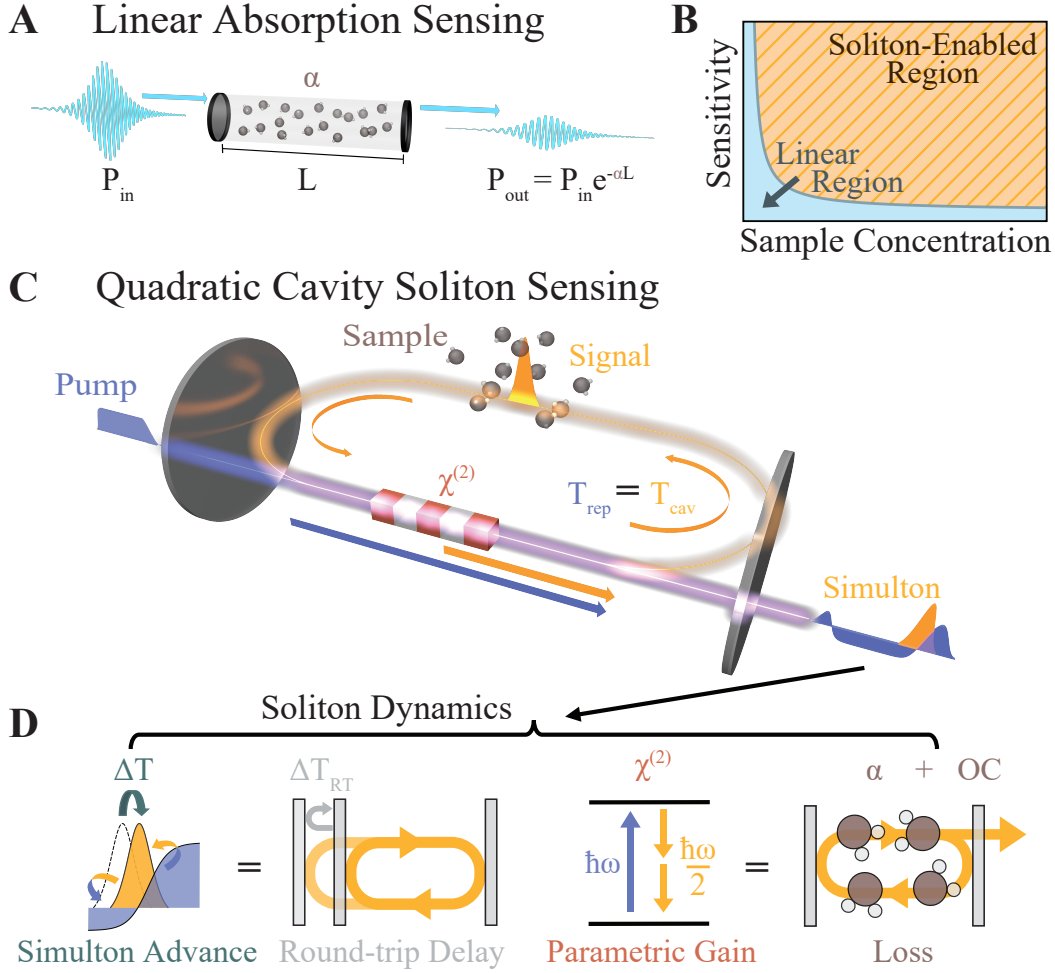


Figure 1: Overcoming the sensitivity vs. dynamic range trade-off imposed by the Beer-Lambert Law using quadratic cavity solitons. (A) Schematic representation of linear absorption sensing governed by the Beer-Lambert Law for light interacting with a sample over a path length L . (B) Linear methods (light blue region) face a fundamental limit in dynamic range, with high sensitivities being difficult to achieve at large sample concentrations. In contrast, active cavity sensing with quadratic cavity solitons (orange) can achieve high sensitivities at large sample concentrations. (C) Schematic depiction of quadratic cavity soliton sensing in the simulton regime of a synchronously-pumped optical parametric oscillator at degeneracy. The bright soliton in the signal interacts with the sample every round-trip, and the resulting competing nonlinear dynamics (D) generate the signal response measured at the output. Specifically, stable simulton operation requires the simulton acceleration leading to a temporal advancement, ΔT , due to gain saturation in the crystal to balance the round-trip delay, ΔT_{RT} , and the parametric gain to balance the sample loss, α , and output coupling. T_{cav} , cavity round-trip time; T_{rep} , pump repetition period; ΔT , simulton group advance; ΔT_{RT} , round-trip delay; ω , angular frequency; α , absorption coefficient; OC, output coupling; P_{in} , input power; P_{out} , output power; L , path length; \hbar , reduced Planck's constant.

[41, 30, 37, 21]. Compared to the multi-mode case, this method can be particularly useful for sensing as the output can be measured with a single detector, alleviating the need for performing spectrally resolved measurements. Additionally, unlike linear absorption sensing, the regime of high sensitivity can be adjusted through variation in the pump rate, enabling higher dynamic range for the measurement.

Despite these advantages, such laser-based sensing systems have limitations in sensitivity imposed by spontaneous emission and difficulty in measuring the low signal powers required for near-threshold operation, in part due to increasing laser instability as threshold is approached [5]. Additional practical difficulties can arise from the spectral availability of narrow-band laser gain media in the region of interest for a given sensing application.

Optical parametric oscillators (OPOs) have also been proposed as a promising candidate for intracavity molecular sensing and spectroscopy due to their large, broadband gain and flexibility in spectral coverage as well as their comparatively low rate of spontaneous emission [9]. However, experimental implementations in the pulsed and quasi-continuous wave regimes have remained far from theoretical predictions due to technological challenges which limit performance of continuous-wave OPOs and a lack of understanding of the nonlinear dynamics of pulsed OPOs [4, 8, 18].

Here, we utilize the formation dynamics of recently-discovered quadratic cavity solitons in OPOs, i.e. temporal solitons, for molecular sensing [20]. Such dynamics enable a fundamentally different sensing scheme that can break many of the limitations of current techniques to achieve high sensitivity, large signal enhancement, and considerable dynamic range for mid-infrared gas sensing while avoiding the typical requirements of high-finesse and high-power operation. Moreover, solitons can be achieved at arbitrary wavelengths, paving the way towards a universal molecular sensing scheme, especially in wavelength ranges where lasers are not readily available. In a proof-of-principle measurement performed on CO₂ in an OPO at 4.18

μm [25], we measure an equivalent path length enhancement as high as 2491 close to threshold and additionally show a maximum sensitivity of 4.1 mW/ppm even at concentrations of CO_2 as high as atmospheric levels. As illustrated in Fig. 1b, this sensitivity of the simulton at large gas concentrations (orange) is shown to be orders of magnitude larger than what can theoretically be achieved through linear methods (light blue) using a probe of equivalent power and bandwidth to the output of our broadband OPO. Furthermore, we theoretically investigate the unique dynamics responsible for this outstanding performance.

The cavity-soliton-based sensing mechanism relies on the extremely high sensitivity of OPO operation in the soliton regime to gain and loss. Figure 1c shows the schematic of such a sensor based on insertion of a gas sample of interest into a doubly-resonant, synchronously pumped OPO around degeneracy. The OPO consists of an optical resonator with a quadratic nonlinearity, which provides the parametric gain. At degeneracy, the nonlinear interaction is phase-matched such that the generated signal and idler light is at the half-harmonic of the pump [28]. Synchronous pumping occurs when the pump repetition period, T_{rep} , is matched to the effective signal round-trip time in the cavity while doubly-resonant operation means the OPO permits the signal and idler to resonate in the cavity while the pump is coupled out. In this way, the degenerate signal which resonates in the cavity will experience absorption from the sample followed by gain from the pump through the parametric process in each round trip.

While OPOs have been successfully used for frequency comb generation in the mid-IR[29, 31], it was more recently shown that they can be designed to support formation of solitons, known as cavity simultons[20, 25]. Simultons are bright-dark soliton pairs of the signal at frequency ω and pump at 2ω , which were initially discovered in traveling-wave configurations [1, 38]. Cavity simultons occur in synchronously-pumped degenerate OPOs in the high-gain, low-finesse regime when a round trip delay is added with respect to conventional operation, meaning the cold cavity time, T_{cav} , is increased with respect to the pump repetition period,

T_{rep} [20]. As depicted in Fig. 1d, stable cavity soliton formation requires a double-balance of energy and timing in which the gain must equal the loss and the soliton group advance, ΔT , which occurs as the signal depletes the pump through the nonlinear interaction in the $\chi^{(2)}$ crystal, must compensate the round-trip delay, ΔT_{RT} , to reestablish synchrony with the pump pulses. The reliance of the timing advance on pump depletion couples the two conditions, as the gain must therefore be sufficiently large for the timing condition to be satisfied, leading to a characteristically strong response to changes in the gain and loss for the soliton near threshold (see Supplementary Information Section 6).

In sharp contrast to other active-cavity schemes, the cavity-soliton-based sensing mechanism, illustrated in Fig. 2, exploits the interplay between energy and timing in the soliton regime to attain high sensitivity to the sample of interest. This extraordinary sensitivity can be explained from the distinctively large threshold and high slope efficiency of the soliton, as depicted in Fig. 2a. For a given pump power, the addition of a small amount of loss due to the sample causes a threshold increase, resulting in a corresponding decrease in the output power, ΔP . The absolute change in power is proportional to the local slope efficiency at the sensing point, meaning a higher slope efficiency results in a higher sensitivity.

In such a scenario, the corresponding path length enhancement is given by:

$$\frac{L_{\text{eff}}}{L} = \frac{-1}{L\Delta\alpha} \ln \left(\frac{P_{\text{signal}}(\alpha + \Delta\alpha)}{P_{\text{signal}}(\alpha)} \right), \quad (1)$$

where L_{eff} is the effective path length, L is the cavity round-trip length, P_{signal} is the signal power, α is the sample absorption coefficient, and $\Delta\alpha$ represents some small change in the absorption due to the addition of sample. Simplified models using single-mode laser theory or continuous-wave OPO theory show the path length enhancement to asymptotically approach infinity as the number of times above threshold, N , approaches unity, as shown schematically in Fig. 2b (see Supplementary Information Sections 4 and 5) [5].

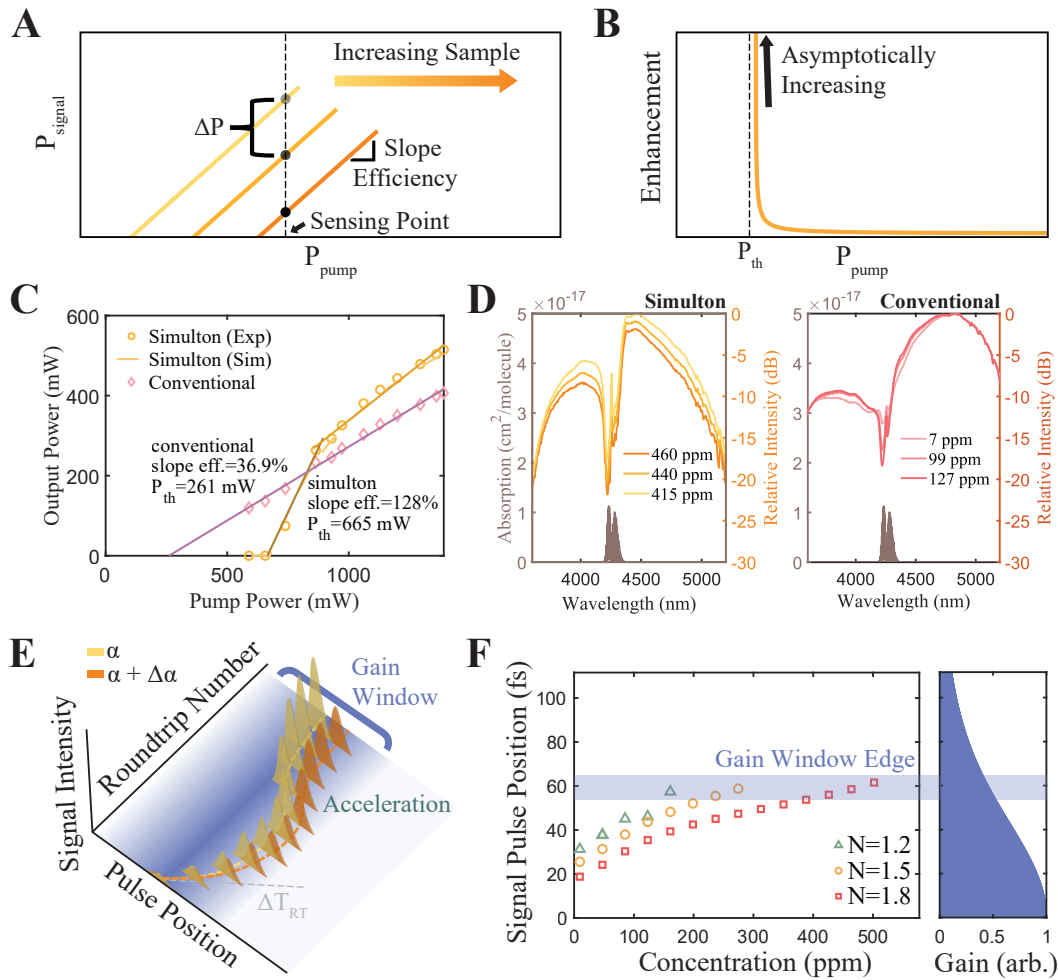


Figure 2: **Quadratic cavity soliton sensing mechanism.** (A) In near-threshold sensing, the addition of sample causes an increase in threshold, resulting in a decrease in signal power at the sensing point. (B) The corresponding signal enhancement grows asymptotically as threshold is approached. (C) Measured input-output power relationships for the simulton (orange) and conventional (pink) regimes show the extremely high slope efficiency and high threshold of the simulton, suggesting its potential for near-threshold sensing with high SNR. Solid lines capture the trends through linear fits of the experimental data while the orange, dashed line shows the corresponding simulton simulation. (D) Experimental power spectral densities demonstrate reduced power across the entire simulton spectrum (left) with the addition of sample despite the relatively narrow absorption feature of the CO_2 , in sharp contrast to the conventional regime (right) and other general multi-mode laser operation. This highlights the importance of simulton formation dynamics for enhanced near-threshold sensing in spite of the broad simulton bandwidth. (E) Schematic depiction of the temporal dynamics of cavity soliton formation which enable the sensing enhancement mechanism. Additional loss in the round-trip limits the ability of the simulton to deplete the pump and accelerate, leading to a reduced gain for all modes at steady-state. (F) Simulated steady-state pulse position as a function of gas concentration (left). Comparison with the theoretical gain window (right) shows the simulton moving further towards the gain window edge as the sample concentration is increased, in accordance with (E).

This large enhancement near threshold is fundamentally followed by a decrease in the signal-to-noise ratio (SNR). However, the combination of large slope efficiency, high threshold, and low spontaneous emission rate of the OPO in the soliton regime makes this SNR reduction extremely slow (see Supplementary Information Sections 4 and 5). As an example, in our experiments (see Supplementary Section 1), the measured soliton threshold is approximately a factor of 2.5 larger than that of the conventional regime, and the slope efficiency is a factor of 3.5 larger, as illustrated in Fig. 2c. The net result is an ability to operate nearly 9 times closer to threshold in the soliton regime at the same output power for detector-limited measurements. This ability to achieve measurable signals very near to the soliton threshold can lead to an extremely large enhancement, making the soliton an ideal candidate for intracavity sensing.

From the fundamental perspective, such cavity-soliton-enhanced sensing cannot be achieved in a general multi-mode laser or conventional OPO as other modes which do not experience the absorption will compensate for the loss in the absorbing modes, leading to a limited change in the laser threshold or output power with the addition of the sample [5]. This is true for conventional sync-pumped OPOs but not for the soliton regime, as shown in Fig. 2d. Here, the experimental spectrum data in both the soliton (left) and conventional (right) regimes is given for three different intracavity CO₂ concentrations. Unlike the conventional regime, the power in all the spectral modes of the soliton regime decreases nearly uniformly with the addition of even a narrow-band sample, mimicking that of a single-mode sensor for which threshold sensing is possible. In contrast to single-mode lasers, however, the soliton enhancement provides broadband operation, which relaxes the requirement for fine tuning of the laser line to a single absorption line, it provides SNR advantages, and it can be achieved in wavelength ranges that are typically not easy to reach with lasers, particularly in the infrared.

Figure 2e schematically depicts the formation of the soliton pulses over multiple round-trips

in the resonator for two different values of the absorption. Due to the round-trip delay, ΔT_{RT} , the newly formed pulse slowly falls out of the gain window, determined by the pump pulse and walk-off length, until it has grown enough to experience a sufficiently strong nonlinear acceleration to compensate the delay. The addition of a small amount of loss in the round-trip to the signal will reduce the amount of acceleration and, correspondingly, the amount of gain experienced by all spectral modes of the simulton super-mode at steady-state as it interacts with the pump in the nonlinear crystal, leading to a spectrally uniform reduction of power despite the relatively narrow absorption spectrum, as shown in the measured spectrum of Fig. 2d.

This dynamical behavior is confirmed through our simulation. Figure 2f depicts the steady-state signal pulse position as a function of CO_2 concentration (left) in comparison to the available gain (right) for three different number of times above threshold, $N=1.2$ (green triangles), $N=1.5$ (orange circles), and $N=1.8$ (red squares). The gain here is calculated as the convolution between the pump pulse shape and the walk-off, with the center of the gain window positioned at 0 fs. The approximate gain window edge can be calculated by halving the sum of the pump pulse length and the walk-off length. Further details can be found in Supplementary Information Section 2. As sample is added to the cavity, the steady-state position of the signal pulse moves towards the gain window edge due to the reduced acceleration of the simulton until it no longer experiences sufficient gain to resonate. This sharp reduction in gain as sample is added to the cavity can enable a high sensitivity for the simulton near threshold.

Figure 3a depicts the measured simulton output power as the CO_2 concentration in the cavity is varied. Green triangles, orange circles, and red squares correspond to pumping at different number of times above threshold (here, $N = 1.25, 1.64,$ and $1.84,$ respectively). Similar to the input-output power dependence shown previously, the output power dependence on CO_2 changes most sharply close to threshold. Solid lines show linear fits of the near-threshold data. Their slope is used to find the sensitivity, with the highest fitted sensitivity calculated to be 4.1

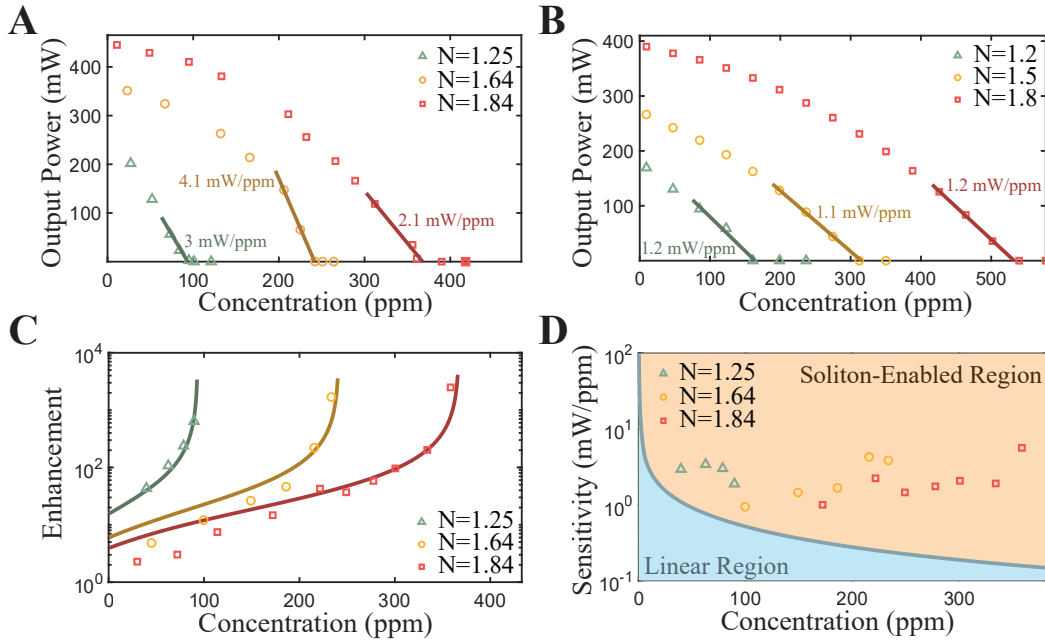


Figure 3: **Sensing behaviors of the quadratic cavity solitons.** (A) Measured output power as a function of CO₂ concentration for different number of times above threshold, N , demonstrating the tunability of the region of high sensitivity for the method. The high slope efficiency of the soliton close to threshold leads to a high sensitivity of up to 4.1 mW/ppm, emphasized using the solid trend lines. (B) Simulations of the soliton response to the addition of CO₂ at various number of times above threshold exhibit good qualitative agreement with the experimental data. The sensitivity is preserved even for pumps at a different number of times above threshold. (C) Equivalent path-length enhancement calculated for neighboring points in the experiment, showing a measured enhancement as large as 2491. Solid lines show the enhancement corresponding to the linear fits in (B). As expected, the enhancement grows asymptotically as threshold is approached for a given N . (D) Measured sensitivity as a function of CO₂ concentration in direct comparison with linear sensing (light blue), demonstrating the potential for orders of magnitude sensitivity improvement over linear methods at high sample concentrations.

mW/ppm. Additionally, we observe that by tuning the pump power, one can change the region of high sensitivity, enabling a large dynamic range for the system.

These observations are consistent with our simulated sensing results, shown in Fig. 3b. Here, we again see the large sensitivity near threshold and tuning of the sensitive region through variation in the number of times above threshold. The calculated sensitivity is also shown to be consistent across the different pump conditions. Our simulated sensitivity is slightly lower than what is observed experimentally, which we attribute primarily to imperfections in our modeling of the gas response.

We also find the equivalent path length enhancement for the experimental data, as shown in Fig. 3c. To do so, we define $\Delta\alpha_{\text{eff}}$ as the effective absorption coefficient experienced by a pump of the same bandwidth as the simulton which has experienced 1.2m of CO₂ absorption at the reference concentration. Using this, we calculate $\frac{-1}{L\Delta\alpha_{\text{eff}}} \ln \left(\frac{P_{\text{signal}}(\alpha_{\text{eff}} + \Delta\alpha_{\text{eff}})}{P_{\text{signal}}(\alpha_{\text{eff}})} \right)$ for neighboring points in our experimental measurement. Further details on this calculation may be found in Supplementary Information Section 3. The largest enhancement of 2491 is observed near threshold for the case where $N = 1.84$, though similar enhancements are observed near threshold for the other cases. Solid lines show the enhancement corresponding to the linear fits from Fig. 3a in accordance with theory. The close fits near threshold illustrate the nearly asymptotic trend for the enhancement, with deviations at lower sample concentrations coming from the observed saturation of the simulton response far above threshold.

In addition to this measured enhancement, we can make direct comparisons with the sensitivity achievable using linear methods. Figure 3d shows the sensitivity in mW/ppm, calculated for neighboring points in our experimental measurement. Note that through variation of the number of times above threshold, a sensitivity near the measured value of 4.1 mW/ppm may be achieved across all concentrations.

By comparison, we have plotted the sensitivities achievable using linear methods (light blue

region). Here, we model a linear cavity with a length of 1.2 m pumped by a pulsed source with the same bandwidth as our measured simulton and an average power of 500 mW. We have additionally assumed a path-length-multiplexed approach in which the path length enhancement is varied to achieve the maximum sensitivity at each point, up to an enhancement of 10^6 and corresponding finesse of over 1.5 million, compared to our cavity which has a finesse of 2. We believe this to be a large enough enhancement limit for linear methods to represent practically achievable values of the finesse. As expected theoretically, an inverse scaling is observed for this path-length-multiplexed approach, emphasizing the limitations in dynamic range of linear techniques. In contrast, the nearly constant and orders of magnitude higher sensitivity demonstrated by the simulton sensing mechanism at large sample concentrations illustrates the potential for this regime to break the trade-off between sensitivity and dynamic range faced by linear methods, which can benefit many applications while avoiding the typical requirements of high-finesse cavities.

The remarkable sensing performance of the simulton could be further improved in several ways. Here, we have only explored the first simulton due to limitations in our pump power, but OPOs will often exhibit multiple simulton resonances as the cavity length is further increased. These further-detuned simultons can exhibit even higher slope efficiencies, leading to potentially larger sensitivities and sensitivity enhancements [20]. Additionally, simultons benefit from operation in the high-gain, low-finesse regime. Recent advances in thin-film lithium niobate nanophotonics, where gains as large as 100 dB/cm have been demonstrated, could push OPOs even further into this regime, enabling the creation of high-sensitivity, highly scalable molecular sensors [24, 23]. Finally, other nonlinear behaviors in OPOs such as spectral phase transitions offer additional means to achieve high sensitivity for intracavity sensing in OPOs [34]. Exploration of different operation regimes of OPOs for multi-species molecular sensing will be the subject of future work [42].

In summary, we have proposed and demonstrated a mid-infrared molecular sensing mechanism which benefits from the nonlinear dynamics of quadratic cavity soliton formation in optical parametric oscillators to simultaneously achieve high sensitivity and large dynamic range. Our proof-of-principle experimental demonstration measuring CO₂ in an OPO at 4.18 μm and complementary simulations show a path length enhancement of 2491 and orders of magnitudes sensitivity enhancement when compared to linear methods at large gas concentrations. This sensitivity enhancement breaks the fundamental sensitivity limitations imposed by the Beer-Lambert Law. Such a sensor could benefit a wide variety of applications, particularly where precise measurement of a wide range of concentrations is required.

References

- [1] S. Akhmanov, A. Chirkin, K. Drabovich, A. Kovrigin, R. Khokhlov, and A. Sukhorukov. Nonstationary nonlinear optical effects and ultrashort light pulse formation. *IEEE Journal of Quantum Electronics*, 4(10):598–605, 1968.
- [2] J. Altmann, R. Baumgart, and C. Weitkamp. Two-mirror multipass absorption cell. *Applied Optics*, 20(6):995–999, 1981.
- [3] E. Antonov, V. Koloshnikov, and V. Mironenko. Quantitative measurement of small absorption coefficients in intracavity absorption spectroscopy using a cw dye laser. *Optics Communications*, 15(1):99–103, 1975.
- [4] A. A. Babin, V. N. Petryakov, and G. Freidman. Feasibility of using singly resonant parametric oscillators for intracavity infrared spectroscopy. *Soviet Journal of Quantum Electronics*, 11(5):664, 1981.

- [5] V. M. Baev, T. Latz, and P. E. Toschek. Laser intracavity absorption spectroscopy. *Applied Physics B*, 69(3):171–202, 1999.
- [6] M. A. Belkin, M. Lončar, B. G. Lee, C. Pflügl, R. Audet, L. Diehl, F. Capasso, D. Bour, S. Corzine, and G. Höfler. Intra-cavity absorption spectroscopy with narrow-ridge microfluidic quantum cascade lasers. *Optics Express*, 15(18):11262–11271, 2007.
- [7] B. Bernhardt, A. Ozawa, P. Jacquet, M. Jacquey, Y. Kobayashi, T. Udem, R. Holzwarth, G. Guelachvili, T. W. Hänsch, and N. Picqué. Cavity-enhanced dual-comb spectroscopy. *Nature photonics*, 4(1):55–57, 2010.
- [8] K.-J. Boller and T. Schröder. Demonstration of broadband intracavity spectroscopy in a pulsed optical parametric oscillator made of β -barium borate. *JOSA B*, 10(9):1778–1784, 1993.
- [9] W. Brunner and H. Paul. The optical parametric oscillator as a means for intracavity absorption spectroscopy. *Optics Communications*, 19(2):253–256, 1976.
- [10] M. Dong, C. Zheng, D. Yao, G. Zhong, S. Miao, W. Ye, Y. Wang, and F. K. Tittel. Double-range near-infrared acetylene detection using a dual spot-ring herriott cell (dsr-hc). *Optics Express*, 26(9):12081–12091, 2018.
- [11] P. Fjodorow, M. P. Frolov, Y. V. Korostelin, V. I. Kozlovsky, C. Schulz, S. O. Leonov, and Y. K. Skasyrsky. Room-temperature fe: Znse laser tunable in the spectral range of 3.7–5.3 μm applied for intracavity absorption spectroscopy of CO_2 isotopes, CO and N_2O . *Optics Express*, 29(8):12033–12048, 2021.
- [12] P. Fjodorow, O. Hellmig, and V. M. Baev. A broadband Tm/Ho-doped fiber laser tunable from 1.8 to 2.09 μm for intracavity absorption spectroscopy. *Applied Physics B*, 124(4):1–8, 2018.

- [13] A. Foltynowicz, T. Ban, P. Masłowski, F. Adler, and J. Ye. Quantum-noise-limited optical frequency comb spectroscopy. *Physical review letters*, 107(23):233002, 2011.
- [14] G. Gagliardi and H.-P. Loock. *Cavity-enhanced spectroscopy and sensing*, volume 179. Springer, 2014.
- [15] A. Garnache, A. Kachanov, F. Stoeckel, and R. Houdre. Diode-pumped broadband vertical-external-cavity surface-emitting semiconductor laser applied to high-sensitivity intracavity absorption spectroscopy. *JOSA B*, 17(9):1589–1598, 2000.
- [16] D. Gilmore, P. V. Cvijin, and G. Atkinson. Intracavity absorption spectroscopy with a titanium: sapphire laser. *Optics communications*, 77(5-6):385–389, 1990.
- [17] A. Goldman and S. Cheskis. Intracavity laser absorption spectroscopy of sooting acetylene/air flames. *Applied Physics B*, 92(2):281–286, 2008.
- [18] M. W. Haakestad, T. P. Lamour, N. Leindecker, A. Marandi, and K. L. Vodopyanov. Intracavity trace molecular detection with a broadband mid-ir frequency comb source. *JOSA B*, 30(3):631–640, 2013.
- [19] J. Hodgkinson and R. P. Tatam. Optical gas sensing: a review. *Measurement Science and Technology*, 24(1):012004, 2012.
- [20] M. Jankowski, A. Marandi, C. Phillips, R. Hamerly, K. A. Ingold, R. L. Byer, and M. Fejer. Temporal simultons in optical parametric oscillators. *Physical Review Letters*, 120(5):053904, 2018.
- [21] E. Kleist and H. Bettermann. Intracavity absorption measurements from liquid samples in an ar+-ion laser. *Optics letters*, 13(6):449–451, 1988.

- [22] J. Langridge, T. Laurila, R. Watt, R. Jones, C. Kaminski, and J. Hult. Cavity enhanced absorption spectroscopy of multiple trace gas species using a supercontinuum radiation source. *Optics Express*, 16(14):10178–10188, 2008.
- [23] L. Ledezma, A. Roy, L. Costa, R. Sekine, R. Gray, Q. Guo, R. M. Briggs, and A. Marandi. Widely-tunable optical parametric oscillator in lithium niobate nanophotonics. *arXiv preprint arXiv:2203.11482*, 2022.
- [24] L. Ledezma, R. Sekine, Q. Guo, R. Nehra, S. Jahani, and A. Marandi. Intense optical parametric amplification in dispersion-engineered nanophotonic lithium niobate waveguides. *Optica*, 9(3):303–308, Mar 2022.
- [25] M. Liu, R. M. Gray, A. Roy, K. A. Ingold, E. Sorokin, I. Sorokina, P. G. Schunemann, and A. Marandi. High-power mid-ir few-cycle frequency comb from quadratic solitons in an optical parametric oscillator. *Laser & Photonics Reviews*, 16(11):2200453, 2022.
- [26] B. Löhden, S. Kuznetsova, K. Sengstock, V. Baev, A. Goldman, S. Cheskis, and B. Pálsdóttir. Fiber laser intracavity absorption spectroscopy for in situ multicomponent gas analysis in the atmosphere and combustion environments. *Applied Physics B*, 102(2):331–344, 2011.
- [27] X. Lou, Y. Feng, S. Yang, and Y. Dong. Ultra-wide-dynamic-range gas sensing by optical pathlength multiplexed absorption spectroscopy. *Photonics Research*, 9(2):193–201, 2021.
- [28] A. Marandi, K. A. Ingold, M. Jankowski, and R. L. Byer. Cascaded half-harmonic generation of femtosecond frequency combs in the mid-infrared. *Optica*, 3(3):324–327, 2016.

- [29] A. Marandi, N. C. Leindecker, V. Pervak, R. L. Byer, and K. L. Vodopyanov. Coherence properties of a broadband femtosecond mid-ir optical parametric oscillator operating at degeneracy. *Optics express*, 20(7):7255–7262, 2012.
- [30] P. Melentiev, A. Kalmykov, A. Gritchenko, A. Afanasiev, V. Balykin, A. Baburin, E. Ryzhova, I. Filippov, I. Rodionov, I. Nechepurenko, et al. Plasmonic nanolaser for intracavity spectroscopy and sensorics. *Applied Physics Letters*, 111(21):213104, 2017.
- [31] A. Muraviev, V. Smolski, Z. Loparo, and K. Vodopyanov. Massively parallel sensing of trace molecules and their isotopologues with broadband subharmonic mid-infrared frequency combs. *Nature Photonics*, 12(4):209–214, 2018.
- [32] A. O’Keefe and D. A. Deacon. Cavity ring-down optical spectrometer for absorption measurements using pulsed laser sources. *Review of scientific instruments*, 59(12):2544–2551, 1988.
- [33] M. A. Reber, Y. Chen, and T. K. Allison. Cavity-enhanced ultrafast spectroscopy: ultrafast meets ultrasensitive. *Optica*, 3(3):311–317, 2016.
- [34] A. Roy, S. Jahani, C. Langrock, M. Fejer, and A. Marandi. Spectral phase transitions in optical parametric oscillators. *Nature communications*, 12(1):1–9, 2021.
- [35] A. Stark, L. Correia, M. Teichmann, S. Salewski, C. Larsen, V. Baev, and P. Toschek. Intracavity absorption spectroscopy with thulium-doped fibre laser. *Optics communications*, 215(1-3):113–123, 2003.
- [36] M. J. Thorpe, K. D. Moll, R. J. Jones, B. Safdi, and J. Ye. Broadband cavity ringdown spectroscopy for sensitive and rapid molecular detection. *Science*, 311(5767):1595–1599, 2006.

- [37] F. Träger, R. Neumann, J. Kowalski, and G. z. Putlitz. Intracavity atomic beam laser spectrometer for low intensity spectral lines. *Applied physics*, 12(1):19–22, 1977.
- [38] S. Trillo. Bright and dark simultons in second-harmonic generation. *Optics letters*, 21(15):1111–1113, 1996.
- [39] B. Tuzson, M. Mangold, H. Looser, A. Manninen, and L. Emmenegger. Compact multi-pass optical cell for laser spectroscopy. *Optics letters*, 38(3):257–259, 2013.
- [40] Z. Yang, T. Albrow-Owen, W. Cai, and T. Hasan. Miniaturization of optical spectrometers. *Science*, 371(6528):eabe0722, 2021.
- [41] Y. Zhang, M. Zhang, W. Jin, H. Ho, M. Demokan, B. Culshaw, and G. Stewart. Investigation of erbium-doped fiber laser intra-cavity absorption sensor for gas detection. *Optics Communications*, 232(1-6):295–301, 2004.
- [42] S. Zhou, R. Gray, M. Liu, A. Roy, and A. Marandi. Towards gas sensing without spectroscopy using mid-infrared optical parametric oscillators. In *Optical Sensors*, pages SM1E–1. Optica Publishing Group, 2022.
- [43] M. A. Zondlo, M. E. Paige, S. M. Massick, and J. A. Silver. Vertical cavity laser hygrometer for the national science foundation gulfstream-v aircraft. *Journal of Geophysical Research: Atmospheres*, 115(D20), 2010.

Acknowledgments

The authors gratefully acknowledge support from AFOSR award FA9550-20-1-0040, NSF Grant No. 1846273, the Center for Sensing to Intelligence at Caltech, and NASA/JPL. R.M.G. is thankful for support from the NSF Graduate Research Fellowship Program (GRFP).

Author Contributions: R.M.G. and A.M. conceived the idea and designed the experiments. R.M.G., S.Z., and M.L. performed the experiments. R.M.G. performed numerical simulations with help from A.R. R.M.G. performed theoretical analysis with help from A.R., L.L., and M.L. R.M.G. and A.M. wrote the manuscript with input from all authors. A.M. supervised the project.

Competing Interests: R.M.G., S.Z., M.L., A.R., and A.M. are inventors on a provisional patent application filed by the California Institute of Technology based in part on the work presented here.

Data Availability: The data used for generation of the figures within this manuscript and other findings of this study are available upon request from the corresponding author.

Code Availability: The code used for simulation and plotting of results is available upon request from the corresponding author.